

Backtracking activation impacts the criticality of excitable networks

Renquan Zhang and Guoyi Quan

School of Mathematical Sciences, Dalian University of Technology, Dalian 116024, China

Jiannan Wang*

Research Institute of Frontier Science,

Beihang University, Beijing 100191, China

Key Laboratory of Mathematics Informatics

Behavioral Semantics, Ministry of Education, China

Sen Pei[†]

Department of Environmental Health Sciences, Mailman School of Public Health,

Columbia University, New York, NY 10032, USA

Abstract

Networks of excitable elements are widely used to model real-world biological and social systems. The dynamic range of an excitable network quantifies the range of stimulus intensities that can be robustly distinguished by the network response, and is maximized at the critical state. In this study, we examine the impacts of backtracking activation on system criticality in excitable networks consisting of both excitatory and inhibitory units. We find that, for dynamics with refractory states that prohibit backtracking activation, the critical state occurs when the largest eigenvalue of the weighted non-backtracking (WNB) matrix for excitatory units, λ_{NB}^E , is close to one, regardless of the strength of inhibition. In contrast, for dynamics without refractory state in which backtracking activation is allowed, the strength of inhibition affects the critical condition through suppression of backtracking activation. As inhibitory strength increases, backtracking activation is gradually suppressed. Accordingly, the system shifts continuously along a continuum between two extreme regimes – from one where the criticality is determined by the largest eigenvalue of the weighted adjacency matrix for excitatory units, λ_W^E , to the other where the critical state is reached when λ_{NB}^E is close to one. For systems in between, we find that $\lambda_{NB}^E < 1$ and $\lambda_W^E > 1$ at the critical state. These findings, confirmed by numerical simulations using both random and synthetic neural networks, indicate that backtracking activation impacts the criticality of excitable networks.

Keywords: excitable networks, criticality, backtracking activation, non-backtracking matrix, excitatory-inhibitory networks, dynamic range

* wangjiannan@buaa.edu.cn

† sp3449@cumc.columbia.edu

1. INTRODUCTION

Excitable networks have been used to model a range of phenomena in biological and social systems including signal propagation in neural networks [1–6], information processing in brain networks [7–9], epidemic spread in human population and information diffusion in social networks [10–13]. The collective dynamics of excitable nodes enable the networked system to distinguish stimulus intensities varied by several orders of magnitude, characterized by a large dynamic range in response to external stimuli. In previous studies, it was found that, for a number of excitable network models, the dynamic range is maximized at the critical state [1, 14–17]. As a result, understanding the condition of criticality is essential for improving the performance and functionality of excitable networks.

The critical condition for excitable networks composed of only excitatory nodes has been extensively studied. In homogeneous random networks, the critical state corresponds to a unit branching ratio [1]. For more general network structures, the criticality for dynamics without refractory state is characterized by the unit largest eigenvalue of the weighted adjacency matrix [14]. More recently, it was shown that for dynamics with refractory states, the critical state is governed by the largest eigenvalue of the weighted non-backtracking (WNB) matrix [17]. In these studies, the largest eigenvalue of the weighted adjacency matrix or WNB matrix is used to define the critical state of excitable networks. However, when inhibitory nodes are introduced, it is unclear how criticality is related to the largest eigenvalues of these two matrices.

In this study, we explore the critical condition of excitable networks consisting of both excitatory (E) and inhibitory (I) nodes. Inhibition presents in many real-world systems and plays a critical role in model dynamics and functions [18–23]. For instance, the introduction of inhibitory nodes into an excitable network operating near the critical state leads to self-sustained network activity [22], and inhibitory connectivity may be essential in maintaining long-term information storage in volatile cortex [23]. In order to elucidate the relationship between criticality and the largest eigenvalues of the weighted adjacency matrix and WNB matrix, we study an excitatory-inhibitory (EI) network model equipped with a threshold-like activation rule [22]. Specifically, we focus on the impact of backtracking activation paths on the critical condition.

We first analyze the model dynamics of EI networks in two extreme conditions where

backtracking activation is allowed without restrictions or entirely prohibited. We find that, in the former case, the critical state is better characterized by the largest eigenvalue of the weighted adjacency matrix for excitatory nodes, λ_W^E , while in the latter case, the criticality is more related to the largest eigenvalue of the WNB matrix for excitatory nodes, λ_{NB}^E . For EI models with refractory states that preclude backtracking activation, the critical state is achieved when λ_{NB}^E is close to one. For EI models without refractory state (i.e., with only resting and excited states), however, the analytical form of the critical condition becomes intractable. We show that, qualitatively, the system gradually shifts from the former case to the latter case as the strength of inhibition increases: for negligible inhibition, λ_W^E is closer to one at the critical state; for strong inhibition, λ_{NB}^E is closer to one at the critical state; for moderate inhibition, we find $\lambda_{NB}^E < 1$ and $\lambda_W^E > 1$ at the critical state. Using numerical simulations in both random and synthetic networks, we verify that a larger inhibitory strength tends to suppress more backtracking activation, which explains the transition between these two regimes. Our findings highlight the impact of backtracking activation, a form of dynamical resonance, on the criticality of excitable networks, and may provide new insight into the study of similar dynamical processes in networked systems.

2. MATERIALS AND METHODS

A. The excitable network model

We consider excitable networks consisting of both excitatory (E) and inhibitory (I) nodes [22]. Contrary to the function of excitatory nodes, the effect of inhibitory nodes is to decrease the activation probability of their neighbors once they are activated. In a network with N nodes, we use $s_i(t)$ to represent the state of node i at time t . Both types of nodes can be in one of $m + 1$ states: the resting state $s_i(t) = 0$, the excited state $s_i(t) = 1$, and refractory states $s_i(t) = 2, 3, \dots, m$. At each discrete time t , a resting node can be activated by an external stimulus with a probability η , or activation propagation from its neighbors independently. Specifically, the signal input strength from a node j to a neighboring node i , denoted by a_{ij} , satisfies $a_{ij} > 0$ if node j is excitatory and $a_{ij} < 0$ if node j is inhibitory. If node j and node i are not connected in the network, we set $a_{ij} = 0$. The weighted adjacency matrix $A = \{a_{ij}\}_{N \times N}$ thus fully describes the network structure as well

as the signal input strength between all pairs of nodes. If a resting node i is not activated by the external stimulus, its activation probability in the next time step $t + 1$ is calculated by summing inputs from all neighbors through a transfer function $\sigma(\cdot)$:

$$s_i(t + 1) = 1 \text{ with probability } \sigma \left(\sum_{j=1}^N a_{ij} \tau(s_j(t)) \right). \quad (1)$$

Here $\sigma(\cdot)$ is a piecewise linear function: $\sigma(x) = 0$ for $x \leq 0$; $\sigma(x) = x$ for $0 < x < 1$; and $\sigma(x) = 1$ for $x \geq 1$. $\tau(\cdot)$ is a characteristic function: when $s_j(t) = 1$, $\tau(s_j(t)) = 1$; otherwise, $\tau(s_j(t)) = 0$. A node can be activated by its neighbors if the net input is positive. Once activated, node i will transit to refractory states deterministically. That is, $s_i(t+1) = s_i(t)+1$ if $1 \leq s_i(t) < m$ and $s_i(t+1) = 0$ if $s_i(t) = m$. Note that, if $m = 1$, there will be no refractory state and the node will directly return to the resting state after activation.

In this study, we use *undirected* networks in which signals can be transmitted in both directions, and assume that the number of E nodes N_e is larger than the number of I nodes N_i . Empirical studies on real-world excitable systems reveals that the majority of neural inputs are excitatory [24]. For ease of analysis, we rearrange node indices so that nodes with index $1 \leq i \leq N_e$ are excitatory and the rest are inhibitory. We consider both homogeneous and heterogeneous networks. For homogeneous network structure, we first generate two Erdős-Rényi (ER) random networks consisting of N_e excitatory nodes and N_i inhibitory nodes. Within each network, each pair of nodes is connected with a probability α . We then randomly connect E nodes and I nodes with a probability β . For heterogeneous network structure, two scale-free (SF) networks of E nodes and I nodes with a power-law degree distribution $P(k) \propto k^{-\gamma}$ are generated using the configuration model [25]. These two networks are then connected by randomly linking E nodes and I nodes with a probability β . In other words, networks of same types of nodes are constructed using either an ER model with a pairwise linking probability α or a configuration model for SF networks with a power-law exponent γ . Different types of nodes are connected randomly using a pairwise linking probability β . We assume the absolute values of link weights $|a_{ij}|$ are distributed uniformly within a range, and the effect of inhibitory nodes is solely represented by the connections from I to E nodes.

In real-world excitable systems, the majority of units are excitatory. For instance, in cortex, approximately 20% of neuron inputs are inhibitory [24]. Together with the fact that the inhibitory nodes need to be activated first before their release of inhibitory signals, the

effect of I-I interactions is quite nominal in response to weak external stimuli. In some modeling studies, the I-I interactions were even neglected [26]. In addition, we focus on the relative strength of same-type and cross-type interactions. It would be sufficient to keep one constant and vary the other (i.e., β). Considering these factors, we decided to study the effect of a varying β .

B. Dynamic range and criticality

The dynamic range of an excitable network measures the range of stimulus intensities that are distinguishable based on network response [1]. For a given stimulus intensity $\eta \in (0, 1)$, the network response F is defined as

$$F = \lim_{T \rightarrow \infty} \frac{1}{T} \sum_{t=0}^T S^t, \quad (2)$$

where S^t is the fraction of excited nodes at time t . The response $F(\eta)$ increases monotonically with a growing intensity of external stimulus η in a nonlinear fashion (see figure 1). For a strong stimulus intensity $\eta \rightarrow 1$, the response $F(\eta)$ will saturate and retain at a maximum value $F_{max} = 1/(m + 1)$. For a negligible stimulus intensity $\eta \rightarrow 0$, the minimum response F_0 depends on the state of the excitable system. In subcritical state, $F(\eta)$ is a linear function of η for $\eta \rightarrow 0$, i.e., $F(\eta) \propto \eta$, with $F_0 \rightarrow 0$. At the critical state, F_0 still approaches to zero but the function $F(\eta)$ becomes nonlinear: $F(\eta) \propto \eta^{1/2}$ (see figure 1(a)). The exponent 1/2 is called the Steven's exponent, which characterizes the criticality of the collective dynamics [1, 27]. In supercritical state, the excitation caused by external stimulus can be self-sustained. Therefore, F_0 becomes a positive number.

The dynamic range of an excitable network is defined based on the function $F(\eta)$. In particular, we define dynamic range Δ as

$$\Delta = 10 \log_{10} \frac{\eta_{high}}{\eta_{low}}, \quad (3)$$

where η_{high} and η_{low} are stimulus intensities corresponding to network responses F_{high} and F_{low} (here $F_x = F_0 + x(F_{max} - F_0)$ for $x \in [0, 1]$). In this study, we use $\eta_{0.9}$ and $\eta_{0.1}$, discarding stimuli that are too close to saturation or too weak to be distinguished from F_0 . Previous studies have demonstrated that dynamic range is maximized at the critical state of an excitable system [1, 14]. Without forcing of external stimuli, excitation activity

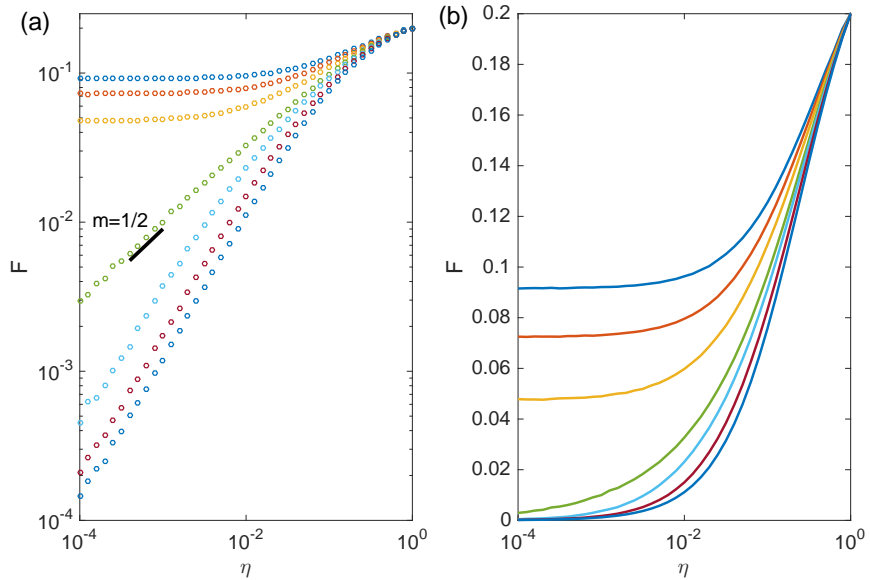


FIG. 1. Network response F in response to external stimulus intensity η . We show the response curves for an EI network constructed by connecting two ER networks ($N_e = 3,000$, $N_i = 2,000$, $\alpha = 3 \times 10^{-3}$, $\beta = 1 \times 10^{-3}$, $m = 4$). The absolute link weights $|a_{ij}|$ are drawn uniformly from 0.1 to 0.2. We multiply link weights with different values to adjust the system to stay in the subcritical, critical and supercritical states. The network response F is shown in logarithmic scale in (a) and linear scale in (b). At the critical state, we show that $F(\eta) \propto \eta^{1/2}$ in (a). The dynamic range of the system is calculated based on the response curve.

will eventually die out in subcritical state but become self-sustained above the critical point. This feature allows us to identify the critical point using the maximization of dynamic range.

The criticality of the proposed model is closely related to percolation. As pointed out in a previous study [28], activation or disease transmission in networks can be mapped to a bond percolation process. In models with only excitatory units, an absorbing state of activation extinction (or a negligible giant component in percolation) exists for a low transmission probability. The criticality of the system corresponds to the transition point of the stability of this absorbing state, which is determined by the branching ratio [1], defined as the average number of secondary activations induced by one excited node. In disease transmission, this quantity is referred to as the reproductive number. If the branching ratio is below one, the absorbing state is stable as all activations eventually die out; in contrast, if the branching ratio is larger than one, the absorbing state becomes unstable and any initial activation will

amplify and converge to a non-zero absorbing state. This stability change is equivalent to the emergence of a non-zero giant component in percolation. The introduction of inhibitory units reduces the transmission probability of activation, thus delays the emergence of a non-zero absorbing state. In particular, inhibitory inputs can be viewed as a means of regulation of the system, and how inhibition is imposed on excitatory units could affect when the stability transition occurs. The phase transition in systems with both excitatory and inhibitory units therefore depends on the competition and interplay between excitatory and inhibitory signals. Depending on whether an excited node can be activated immediately after its last excitation, the effect of inhibitory units is different. This study aims to explore how inhibitory units would change the condition of criticality.

3. RESULTS

The number of refractory states in model dynamics determines whether backtracking activation is permitted. Backtracking activation describes the following phenomenon of dynamical resonance: an excitatory node i activated at time t increases the activation probability of its excitatory neighbors at time $t + 1$, which in turn increases the activation probability of node i at time $t + 2$. This behavior is only possible when there is no refractory state (i.e., $m = 1$) so that excited nodes can directly return to the resting state at time $t + 1$. For dynamics with refractory states (i.e., $m > 1$), nodes excited at time t will enter refractory states at time $t + 1$ thus cannot be activated again at time $t + 2$. Following this dynamical rule, any backtracking activation is prohibited.

A. Dynamics without backtracking activation

We first analyze the simpler case where backtracking is precluded by the existence of refractory states (i.e., $m > 1$). To account for the dynamics without backtracking, we formulate the model evolution in a message-passing framework [17], which is frequently used in statistical physics and network science [29–31]. For a link from i to j ($i \rightarrow j$), we create a “cavity” at node j by “virtually” removing it from the network, and examine the probability of node i being activated in the absence of node j , denoted by $p_{i \rightarrow j}^t$ at time t . The procedure of creating a virtual cavity at node j blocks the backtracking path $i \rightarrow j \rightarrow i$,

and therefore excludes the contribution via the consecutive activation $i \rightarrow j \rightarrow i$ to the activation probability of node i . This framework precisely depicts the model dynamics with refractory states.

For sparse networks without too many short loops, the probabilities $p_{i \rightarrow j}^t$ for neighboring nodes are mutual independent. Under this condition, the probability $p_{i \rightarrow j}^t$ for each node i can be recursively written as follows:

$$p_{i \rightarrow j}^{t+1} = \left(1 - \sum_{l=0}^{m-1} p_{i \rightarrow j}^{t-l}\right) \left[\eta + (1 - \eta) \sigma \left(\sum_{k \in \partial i \setminus j} a_{ik} p_{k \rightarrow i}^t \right) \right]. \quad (4)$$

Here $\partial i \setminus j$ is the set of neighbors of node i excluding j . The probability that node i is excited at time $t + 1$, denoted by p_i^{t+1} , is calculated by putting node j back to the network:

$$p_i^{t+1} = \left(1 - \sum_{l=0}^{m-1} p_i^{t-l}\right) \left[\eta + (1 - \eta) \sigma \left(\sum_{k \in \partial i} a_{ik} p_{k \rightarrow i}^t \right) \right]. \quad (5)$$

Note that, although Eqs (4)-(5) are derived for locally tree-like sparse networks, it has been found that results based on the sparseness assumption work well even for some networks with dense clusters [32].

1. Analysis in the case of negligible inhibition

The piecewise transfer function $\sigma(\cdot)$ imposes a threshold-like activation rule that depends on the collective dynamics of all neighbors. Because the value of net input $\sum_{k \in \partial i \setminus j} a_{ik} p_{k \rightarrow i}^t$ is unknown, it becomes complicated to expand the right-hand-side of Eq (4) except for some extreme cases. Here, we consider a special case where the cross-type interaction β is negligible, i.e., $\beta \rightarrow 0$. Under this extreme condition, excitatory and inhibitory nodes in effect form two nearly separate communities. In particular, inhibitory nodes are unlikely to be activated in response to weak stimuli as they almost only receive signals from inhibitory peers. As a consequence, it is suffice to consider only excitatory nodes to compute network response.

In the steady state, denote the limiting probabilities as $\lim_{t \rightarrow \infty} p_{i \rightarrow j}^t = p_{i \rightarrow j}$ and $\lim_{t \rightarrow \infty} p_i^t = p_i$. For excitatory nodes, Eqs (4)-(5) becomes

$$p_{i \rightarrow j} = (1 - m p_{i \rightarrow j}) \left[\eta + (1 - \eta) \sum_{k \in \partial_E i \setminus j} a_{ik} p_{k \rightarrow i} \right], \quad (6)$$

$$p_i = (1 - mp_i) \left[\eta + (1 - \eta) \sum_{k \in \partial_E i} a_{ik} p_{k \rightarrow i} \right], \quad (7)$$

where $1 \leq i \leq N_e$, $1 \leq j \leq N_e$ and $\partial_E i$ is the set of excitatory neighbors of node i . To solve the self-consistent equations, we introduce two auxiliary variables: $G_{i \rightarrow j}(\eta, p_{\rightarrow}) = \eta + (1 - \eta) \sum_{k \in \partial_E i \setminus j} a_{ik} p_{k \rightarrow i}$, $G_i(\eta, p_{\rightarrow}) = \eta + (1 - \eta) \sum_{k \in \partial_E i} a_{ik} p_{k \rightarrow i}$. We rearrange Eqs (6)-(7) and obtain

$$p_{i \rightarrow j} = \frac{G_{i \rightarrow j}(\eta, p_{\rightarrow})}{mG_{i \rightarrow j}(\eta, p_{\rightarrow}) + 1} \quad (8)$$

and

$$p_i = \frac{G_i(\eta, p_{\rightarrow})}{mG_i(\eta, p_{\rightarrow}) + 1}. \quad (9)$$

For $\eta = 0$ (that is, without external forcing), Eq (8) has a trivial solution: $p_{i \rightarrow j} = 0$ for all links $i \rightarrow j$. The stability of this solution determines the critical state of the system. If the solution is stable, the network activity triggered by a weak stimulus will eventually disappear; otherwise, the response will maintain at a nonzero level.

The stability of the zero solution depends on the Jacobian matrix $\widehat{\mathcal{M}}^E = \{\mathcal{M}_{k \rightarrow l, i \rightarrow j}^E\}$ defined on all pairs of links $k \rightarrow l$ and $i \rightarrow j$ between E nodes. Specifically, we have

$$\begin{aligned} \mathcal{M}_{k \rightarrow l, i \rightarrow j}^E &= \left. \frac{\partial p_{i \rightarrow j}}{\partial p_{k \rightarrow l}} \right|_{\{\eta=0, p_{i \rightarrow j}=0\}} \\ &= \frac{\frac{\partial G_{i \rightarrow j}}{\partial p_{k \rightarrow l}} (mG_{i \rightarrow j} + 1) - mG_{i \rightarrow j} \frac{\partial G_{i \rightarrow j}}{\partial p_{k \rightarrow l}}}{(mG_{i \rightarrow j} + 1)^2} \\ &= \left. \frac{\partial G_{i \rightarrow j}}{\partial p_{k \rightarrow l}} \right|_{\{\eta=0, p_{i \rightarrow j}=0\}}. \end{aligned} \quad (10)$$

Here $G_{i \rightarrow j} = 0$ when $\eta = 0$ and $p_{i \rightarrow j} = 0$ for all $i \rightarrow j$. According to the definition of $G_{i \rightarrow j}$, the partial derivative of $G_{i \rightarrow j}$ is given by

$$\left. \frac{\partial G_{i \rightarrow j}}{\partial p_{k \rightarrow l}} \right|_{\{\eta=0, p_{i \rightarrow j}=0\}} = \begin{cases} a_{lk} & \text{if } l = i \text{ and } j \neq k, \\ 0 & \text{otherwise.} \end{cases} \quad (11)$$

The elements of $\widehat{\mathcal{M}}^E$ are $\mathcal{M}_{k \rightarrow l, i \rightarrow j}^E = a_{lk}$ if $l = i$ and $j \neq k$ and 0 otherwise. Note that, $\mathcal{M}_{k \rightarrow l, i \rightarrow j}^E$ is non-zero only if the links $k \rightarrow l$ and $i \rightarrow j$ are consecutive ($l = i$) but not backtracking ($j \neq k$). The weighted non-backtracking (WNB) matrix, or Hashimoto matrix [33], has recently found applications in several problems in network science [30, 34–40]. Because the stability of the zero solution is determined by the largest eigenvalue λ_{NB}^E of $\widehat{\mathcal{M}}^E$, the system reaches the critical state if $\lambda_{NB}^E = 1$.

2. Numerical results for dynamics with inhibition

For the general case where inhibition cannot be neglected, it is challenging to derive the analytical condition of criticality from Eq (4). As a result, we have to use numerical methods to find the critical state. In particular, we are interested in how the largest eigenvalue of the WNB matrix for E nodes λ_{NB}^E changes with the inhibitory strength β at the critical state. We treat the increasing level of inhibition as a perturbation to the special case of $\beta = 0$, and examine to what extent the critical condition $\lambda_{NB}^E = 1$ will remain valid. In order to tune the system to the critical state, for a fixed inhibitory strength β , we randomly draw absolute link weights $|a_{ij}|$ from a uniform distribution between 0.1 and 0.2, and then multiply $|a_{ij}|$ with a varying constant until the dynamic range of the system is maximized (i.e., the critical state is reached). The largest eigenvalue λ_{NB}^E of $\widehat{\mathcal{M}}^E$ is then computed using a power method [41]. In figure 2, we show the relationship between dynamic range and the largest eigenvalues of four matrices (i.e., the weighted adjacency matrix for all nodes, the weighted non-backtracking matrix for all nodes, the weighted adjacency matrix for E nodes, and the weighted non-backtracking matrix for E nodes). The curves present the largest eigenvalues of different matrices at the critical state where dynamic range is maximized.

We first analyze homogeneous network structure. Without loss of generality, we assume there are 3 refractory states ($m = 4$). For ER networks with $N_e = 3,000$ excitatory nodes and $N_i = 2,000$ inhibitory nodes, we set the within-type connection probability $\alpha = 3 \times 10^{-3}$. An increasing level of inhibitory strength $\beta = 1 \times 10^{-4}, 5 \times 10^{-4}, 1 \times 10^{-3}, 2 \times 10^{-3}$ and 3×10^{-3} are tested. For each β , we slowly tune the link weights to drive the system to the critical state, and record the largest eigenvalue of the WNB matrix for E nodes λ_{NB}^E . We perform 300 realizations of this procedure, and report the distributions of λ_{NB}^E in figure 3. For comparison, we also computed the largest eigenvalue of the weighted adjacency matrix for E nodes λ_W^E at criticality.

Interestingly, even with non-negligible inhibition, λ_{NB}^E consistently distributes around one at the critical state for an increasing inhibitory strength β . In contrast, λ_W^E distributes well above one. We note that the variation of λ_{NB}^E and λ_W^E is attributed to the finite network size and numerical inaccuracy, as pointed out in a previous study on excitable networks with only E nodes [17]. The numerical results in figure 3 indicate that the criticality of EI networks with refractory states occurs when λ_{NB}^E is close to one, regardless of the strength

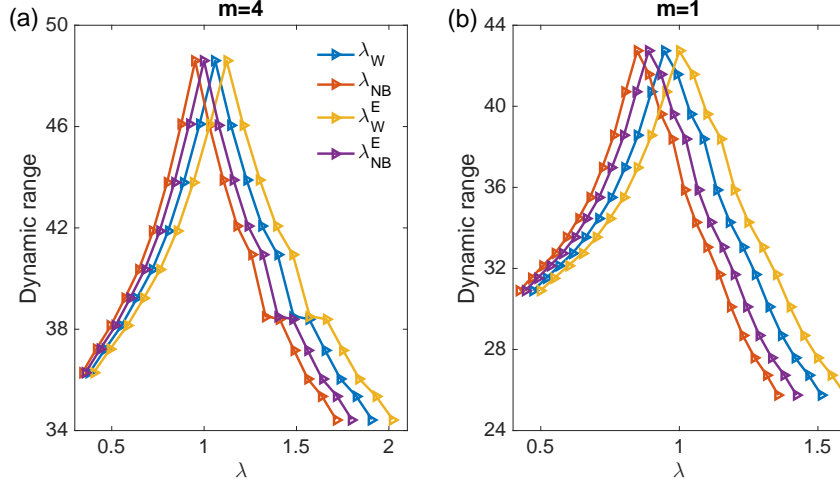


FIG. 2. The relationship between dynamic range and the largest eigenvalues of four matrices for dynamics with 3 refractory states (a) and without refractory state (b). Here, λ_W , λ_{NB} , λ_W^E and λ_{NB}^E are the largest eigenvalues of the weighted adjacency matrix for all nodes, the weighted non-backtracking matrix for all nodes, the weighted adjacency matrix for E nodes, and the weighted non-backtracking matrix for E nodes, respectively. We perform the experiment on an EI network constructed using two ER networks ($N_e = 3,000$, $N_i = 2,000$, $\alpha = 3 \times 10^{-3}$, $\beta = 1 \times 10^{-3}$), and vary link weights to change the state of the system. For each setting of link weights, we calculate the dynamic range and the corresponding largest eigenvalues. The setting that maximizes the dynamic range corresponds to the critical state. We use this numerical method to find the critical state of an EI network. At criticality, we find that λ_{NB}^E is close to one for $m = 4$ and λ_W^E is close to one for $m = 1$. λ_W (λ_{NB}) is always smaller than λ_W^E (λ_{NB}^E) due to the existence of inhibitory nodes.

of inhibition β . A closer inspection of figure 3 reveals that the average value of λ_{NB}^E is slightly larger than one and slowly increases with β . This slight shift of λ_{NB}^E indicates that inhibition does impact the critical condition but its impact is very limited.

According to model dynamics, the function of I nodes is passive – they need to be first activated before they can release inhibition signals. Without external stimuli, the conduction of inhibitory signals proceeds as follows: a set of excited E nodes activate an I node at time t ; at time $t + 1$, the excited I node exerts inhibitory signals to all its neighbors, among which the excited E nodes enter refractory state. With the presence of nodes in refractory state, we hypothesize that the inhibition effect is weakened. To demonstrate this, we plot F_0 as

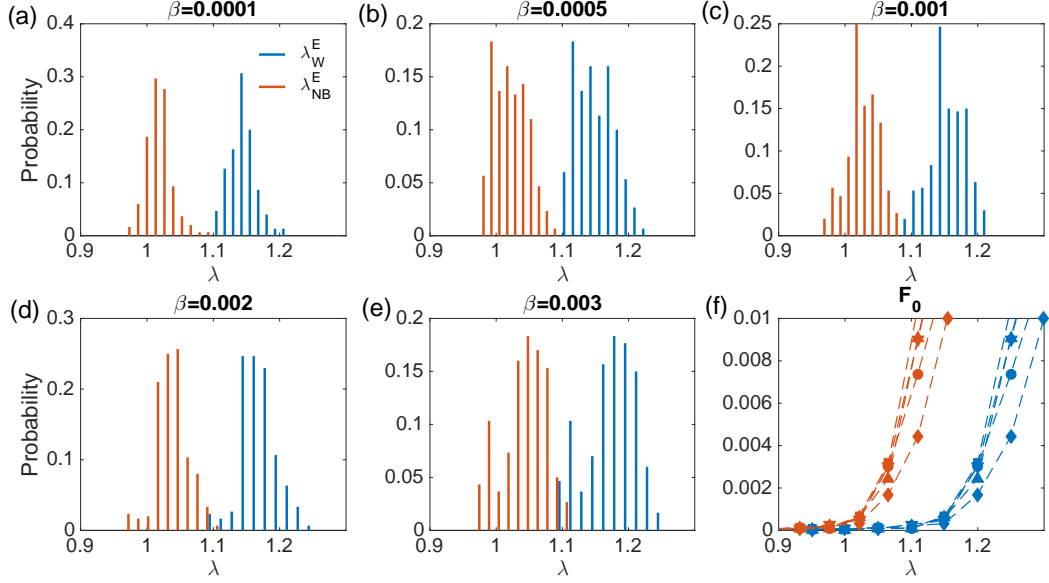


FIG. 3. Distributions of λ_W^E and λ_{NB}^E at the critical state of homogeneous EI networks with refractory states ($m = 4$) (a-e). Networks are constructed by connecting two ER networks ($N_e = 3,000$, $N_i = 2,000$, $\alpha = 3 \times 10^{-3}$), and varying the cross-type link probability β . For different settings of β , λ_{NB}^E is consistently distributed near one. The relationship between F_0 and λ_W^E and λ_{NB}^E is shown in (f) for $\beta = 1 \times 10^{-4}$ (up triangle), 5×10^{-4} (square), 1×10^{-3} (down triangle), 2×10^{-3} (circle), and 3×10^{-3} (diamond). The transition point from $F_0 = 0$ to $F_0 > 0$ is not affected by the strength of inhibition β .

a function of λ_{NB}^E and λ_W^E for increasing β in figure 3(f). Although the inhibitory strength β intensifies, the F_0 curve does not change significantly, especially near the transition point from $F_0 = 0$ to $F_0 > 0$. This result directly shows that, for dynamics with refractory states, the impact of inhibitory nodes is rather limited near the critical state.

We performed the same analysis in SF networks with $N_e = 6,000$, $N_i = 4,000$ and the power-law exponent $\gamma = 3$. Results in figure 4 show that, consistent with the results for ER networks, λ_{NB}^E is close to one at the critical state. The effect of inhibitory nodes near the critical state is also nominal as the F_0 curves are almost identical for different values of inhibitory strength β .

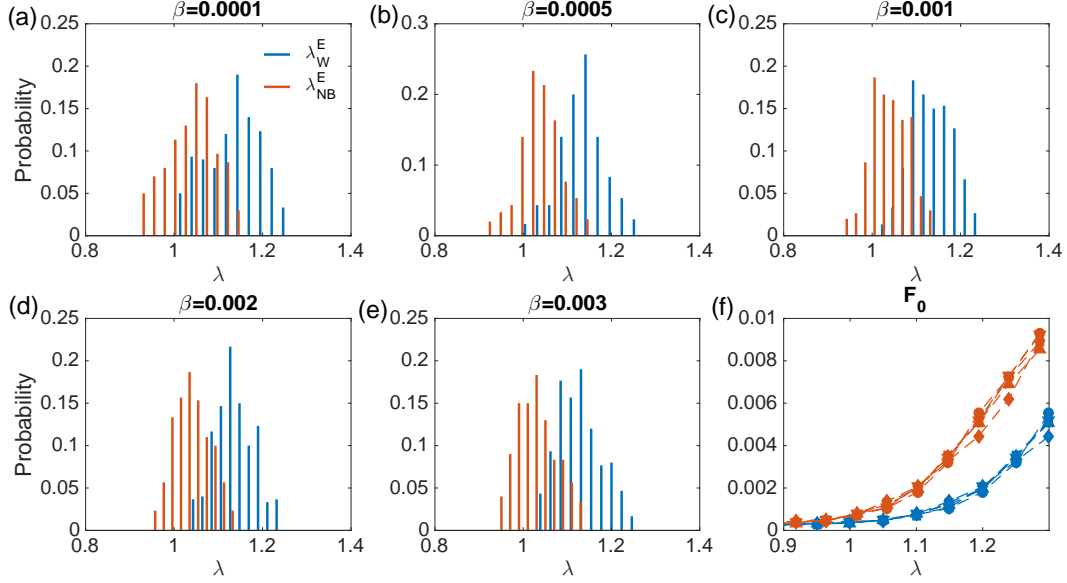


FIG. 4. Distributions of λ_W^E and λ_{NB}^E at the critical state of heterogeneous EI networks with refractory states ($m = 4$) (a-e). Networks are constructed by connecting two SF networks ($N_e = 6,000$, $N_i = 4,000$, $\gamma = 3$), and varying the cross-type link probability β . For different settings of β , λ_{NB}^E is consistently distributed near one. The relationship between F_0 and λ_W^E and λ_{NB}^E is shown in (f) for $\beta = 1 \times 10^{-4}$ (up triangle), 5×10^{-4} (square), 1×10^{-3} (down triangle), 2×10^{-3} (circle), and 3×10^{-3} (diamond). The transition point from $F_0 = 0$ to $F_0 > 0$ is not affected by the strength of inhibition β .

B. Dynamics with backtracking activation

We now explore the more complicated dynamics in which backtracking activation is allowed. In this case, nodes have only two states – resting and excited. For each node i , denote p_i^t as the probability that node i is excited at time t . According to the model dynamics, the evolution of p_i^t is described by

$$p_i^{t+1} = (1 - p_i^t) \left[\eta + (1 - \eta) \sigma \left(\sum_{k=1}^N a_{ik} p_k^t \right) \right]. \quad (12)$$

Backtracking activation is properly represented in Eq (12): if we expand p_k^t on the right-hand-side of Eq (12) in terms of the activation probability at time $t - 1$, p_i^{t+1} becomes explicitly dependent on p_i^{t-1} . This implies, the activation probability of each E node at a given time can contribute to the probability of its re-activation two time-steps later (as

long as at least one of its E neighbors are activated), which exactly depicts the effect of backtracking activation.

1. Analysis in the case of negligible inhibition

Similar with our analysis of dynamics with refractory states, we first explore the extreme case where the cross-type linking probability $\beta \rightarrow 0$. In this case, we only consider the network of excitatory nodes. The stationary activation probability $p_i = \lim_{t \rightarrow \infty} p_i^t$ satisfies

$$p_i = (1 - p_i) \left[\eta + (1 - \eta) \sum_{k=1}^{N_e} a_{ik} p_k \right]. \quad (13)$$

Without external stimuli, the system has a trivial solution $p_i = 0$ for $1 \leq i \leq N_e$. The stability of the zero solution is determined by the largest eigenvalue λ_W^E of the weighted adjacency matrix for excitatory nodes $A^E = \{a_{ij}\}_{N_e \times N_e}$. As a result, the critical state is characterized by $\lambda_W^E = 1$ as $\beta \rightarrow 0$.

2. Numerical results for dynamics with inhibition

We perturb the extreme case $\beta \rightarrow 0$ by gradually increasing the cross-type linking probability β , which introduces more inhibitory nodes connected to excitatory nodes. Without refractory states, an “excitatory→inhibitory→excitatory” feedback loop appears: a group of excited E nodes activate an inhibitory node; the excited I node then releases inhibitory signals and decreases the activation probability of the E nodes who just activated it and now returned to the resting state. The inhibitory signals (negative inputs) impose a threshold for the re-activation of those E nodes. As a consequence, contributions from certain backtracking paths may not be realized. This phenomenon is caused by the threshold-like feature of the transfer function $\sigma(\cdot)$. If the contribution of a backtracking path is lower than the threshold imposed by inhibitory nodes, it may never contribute to the activation probability as $\sigma(x) > 0$ only if the net input $x > 0$. Following this line of reasoning, Eq (13) thus overestimates the effect of backtracking activation when more inhibitory nodes are connected to excitatory nodes. A stronger inhibitory strength β will suppress more backtracking activations, which drives the dynamics of EI networks closer to the opposite extreme case where backtracking activation is entirely prohibited, described by Eqs (6)-(7).

We therefore hypothesize that, for a weak inhibitory strength β , λ_W^E is close to one at the critical state; whereas for a strong inhibitory strength, λ_{NB}^E is close to one at the critical state. Varying the cross-type linking probability β modulates the system shifting between these two extreme regimes. For an intermediate inhibitory strength β , we hypothesize that $\lambda_{NB}^E < 1$ and $\lambda_W^E > 1$ at the critical state. We verify this hypothesis using numerical simulations in both homogeneous and heterogeneous networks.

We performed the same analysis as in figure 3 and figure 4, except using a different model dynamics with only resting and excited states. The distributions of λ_W^E and λ_{NB}^E at the critical state for ER networks is shown in figure 5. In agreement with our hypothesis, as β increases, λ_W^E shifts from near one to above one, and λ_{NB}^E shifts from below one to near one. The same phenomenon is also observed for SF networks in figure 6. In order to examine the effect of inhibitory nodes, we plot the F_0 curve as a function of λ_W^E and λ_{NB}^E in figure 5(f) and figure 6(f). In contrast to dynamics with refractory states, introduction of more inhibitory links effectively reduces F_0 , thus strongly impacts the critical state of the system. Such impact is reflected by the change of the transition point above which F_0 becomes non-zero.

Ideally, it would be desirable to show that the number of instances of backtracking activation decreases with an increasing inhibitory strength β . However, as the activation of a node is collectively determined by a group of nodes, it is difficult to disentangle such interaction and identify definitively which backtracking path is responsible for the activation. Despite that, the impact of inhibitory nodes can be reflected by the threshold values that they impose on excitatory nodes. We calculate the average input from I nodes to E nodes in ER and SF networks. Specifically, for a given stimulus intensity η , we compute the average input of resting E nodes from their excited inhibitory neighbors at each time step, and then average over all time steps. In figure 7(a) and (c), we show that the average threshold indeed increases monotonically with β . In addition, a stronger external stimulus η leads to a higher average threshold due to a larger number of excited nodes.

We further calculate the fraction of excitatory links connected to resting E nodes whose weights are lower than the threshold. To be specific, for each resting E node, we find its excited excitatory neighbors and focus on the links connected to them. These links are potential candidates of backtracking activation, i.e., the actual backtracking activation paths belong to this set of links. Among these links, we calculate the proportion whose weights are

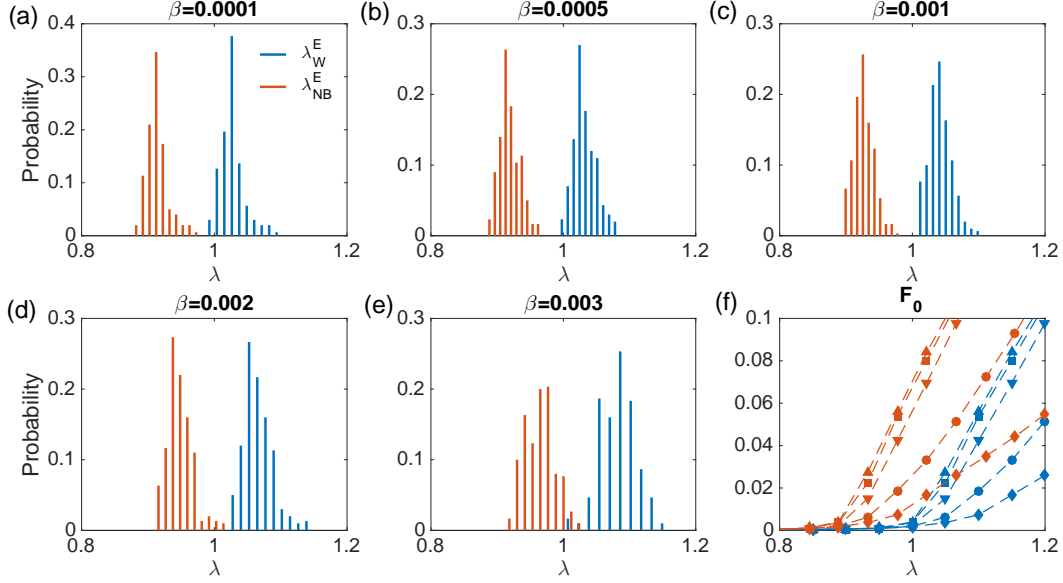


FIG. 5. Distributions of λ_W^E and λ_{NB}^E at the critical state of homogeneous EI networks without refractory state ($m = 1$) (a-e). Networks are constructed by connecting two ER networks ($N_e = 3,000$, $N_i = 2,000$, $\alpha = 3 \times 10^{-3}$), and varying the cross-type link probability β . At the critical state, we show that in general $\lambda_W^E > 1$ and $\lambda_{NB}^E < 1$. As β increases, λ_{NB}^E becomes closer to one and λ_W^E shifts away from one. The relationship between F_0 and λ_W^E and λ_{NB}^E is shown in (f) for $\beta = 1 \times 10^{-4}$ (up triangle), 5×10^{-4} (square), 1×10^{-3} (down triangle), 2×10^{-3} (circle), and 3×10^{-3} (diamond). The transition point from $F_0 = 0$ to $F_0 > 0$ is significantly affected by the strength of inhibition β .

lower than the threshold of the E node. The contribution from such below-threshold links are likely to be negated by the threshold. Therefore, the fraction of below-threshold links can partly reflect the magnitude of backtracking suppression. We present an illustration for computing this below-threshold fraction in figure 8. The mean fraction values averaged over all resting E nodes in all time steps for ER and SF networks are shown in figure 7(b) and (d). For both network structures, the fraction of below-threshold links increases as β grows with the presence of different levels of external stimuli. This analysis agrees with our hypothesis and partially explains the transition between the two extreme cases.

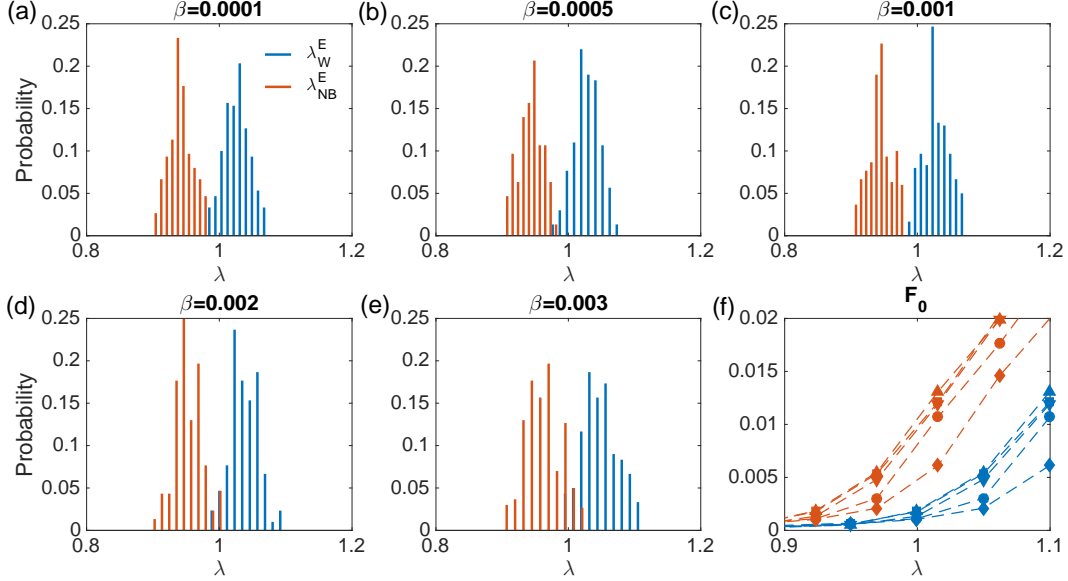


FIG. 6. Distributions of λ_W^E and λ_{NB}^E at the critical state of heterogeneous EI networks without refractory state ($m = 1$) (a-e). Networks are constructed by connecting two SF networks ($N_e = 6,000$, $N_i = 4,000$, $\gamma = 3$), and varying the cross-type link probability β . At the critical state, we show that in general $\lambda_W^E > 1$ and $\lambda_{NB}^E < 1$. As β increases, λ_{NB}^E becomes closer to one and λ_W^E shifts away from one. The relationship between F_0 and λ_W^E and λ_{NB}^E is shown in (f) for $\beta = 1 \times 10^{-4}$ (up triangle), 5×10^{-4} (square), 1×10^{-3} (down triangle), 2×10^{-3} (circle), and 3×10^{-3} (diamond). The transition point from $F_0 = 0$ to $F_0 > 0$ is significantly affected by the strength of inhibition β .

C. Simulations in synthetic neural networks

We further validate our findings in synthetic neural networks that have more realistic structures. As it is difficult to find a real-world neural network dataset that contains both excitatory and inhibitory neurons, we have to construct a synthetic network using network generation models [26, 42, 43]. In particular, networks of neurons in brain follow a clustered, distance-dependent connection pattern [43]. We generate networks with this organizational pattern using a distance-dependent method employed in previous studies [43]. Specifically, 3,000 excitatory nodes and 2,000 inhibitory nodes are placed uniformly on the surface of a unit sphere (figure 9(a)). The degree of each node was generated from a normal distribution. Nodes were then connected according to a distance-dependent probability $P \propto 1/d^2$, where d is the geodesic distance between two nodes on the spherical surface. We assign the synaptic

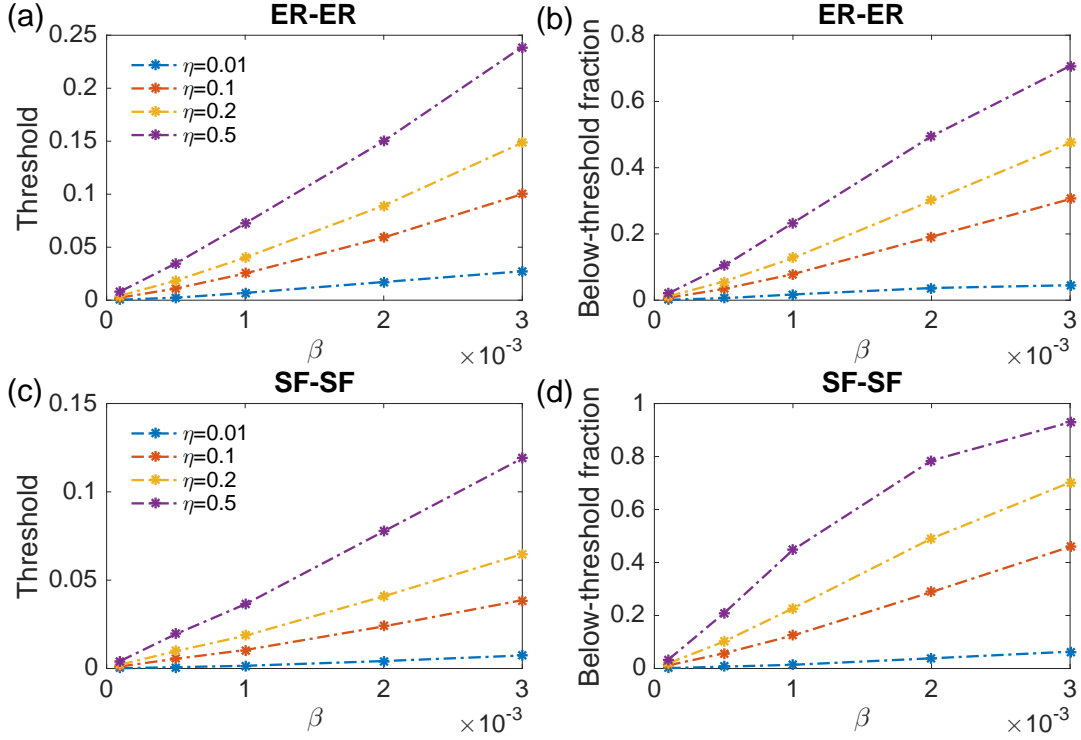


FIG. 7. The threshold of resting E nodes imposed by their inhibitory neighbors for EI networks generated using ER ($N_e = 3,000$, $N_i = 2,000$, $\alpha = 3 \times 10^{-3}$) (a) and SF ($N_e = 6,000$, $N_i = 4,000$, $\gamma = 3$) (c) networks. The fraction of below-threshold links for resting E nodes is reported in (b) and (d). For an increasing level of inhibition strength β , we tune the system to the critical state, and calculate the threshold values and fraction of below-threshold links for different stimulus intensities η . As β and η increase, both threshold and below-threshold fraction increase.

strength of all links from a uniform distribution between 0.1 and 0.2, and multiply a factor c to the weights of cross-type links in order to adjust the strength of inhibition. The value of c reflects the inhibition strength in the system.

We run simulations of model dynamics without refractory state ($m = 1$) for $c = 1$. We vary link weights, and calculate the dynamic range λ_W^E and λ_{NB}^E for each weight setting. The relationship between the dynamic range and λ_W^E and λ_{NB}^E is shown in figure 9(b). Similar with the results in random networks, at the critical state, we find that $\lambda_W^E > 1$ and $\lambda_{NB}^E < 1$. In the inset, we show the values of λ_W^E and λ_{NB}^E at the critical state for an increasing inhibition strength c . As c grows, at the critical state, λ_W^E shifts away from one and λ_{NB}^E gets closer to one. This result further corroborates our hypothesis that the system

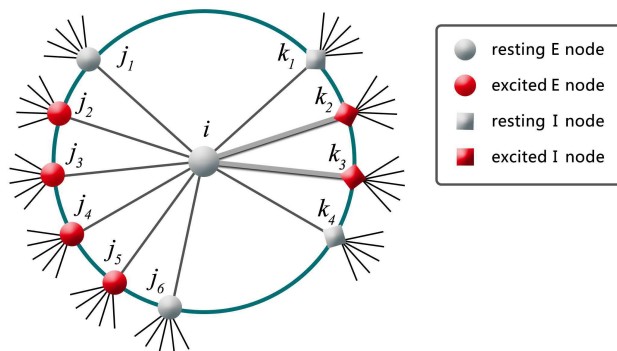


FIG. 8. An example to show the calculation of threshold and fraction of below-threshold links for a resting E node i . Here, the resting E node has a total input $|a_{ik_2} + a_{ik_3}|$ for its activated I neighbors. This value is defined as the threshold. Among the 4 links connected to its activated E neighbors, 2 links have weights below the threshold ($a_{ij_3} < |a_{ik_2} + a_{ik_3}|$, $a_{ij_4} < |a_{ik_2} + a_{ik_3}|$). The fraction of below-threshold links is calculated as $2/4 = 0.5$.

lies between two extremes with ($\lambda_W^E \approx 1$) and without ($\lambda_{NB}^E \approx 1$) backtracking activation.

4. CONCLUSION

In this study, we explore the impact of backtracking activation on the criticality of excitable networks with both excitatory and inhibitory nodes. We find that, for dynamics with refractory state that precludes backtracking activation, the critical state occurs when the largest eigenvalue of the WNB matrix for excitatory nodes is close to one. However, for dynamics without refractory state, the introduction of inhibitory nodes affects backtracking activation and the critical condition of the system. The EI model with inhibition essentially provides an intermediate system between two extreme cases in which backtracking activation is allowed or prohibited. For the dynamics with a medium inhibitory strength, λ_W^E and λ_{NB}^E can be viewed as the upper and lower bound of the critical condition: at the critical state, $\lambda_W^E > 1$ and $\lambda_{NB}^E < 1$. In practice, this criterion can be used to assess whether a system may be at the critical state. If a system resides in a state where $\lambda_W^E < 1$ or $\lambda_{NB}^E > 1$, we can assert that the system is not close to the critical state. Our results imply that a precise description of model dynamics is essential in theoretical analysis of phase transitions. These

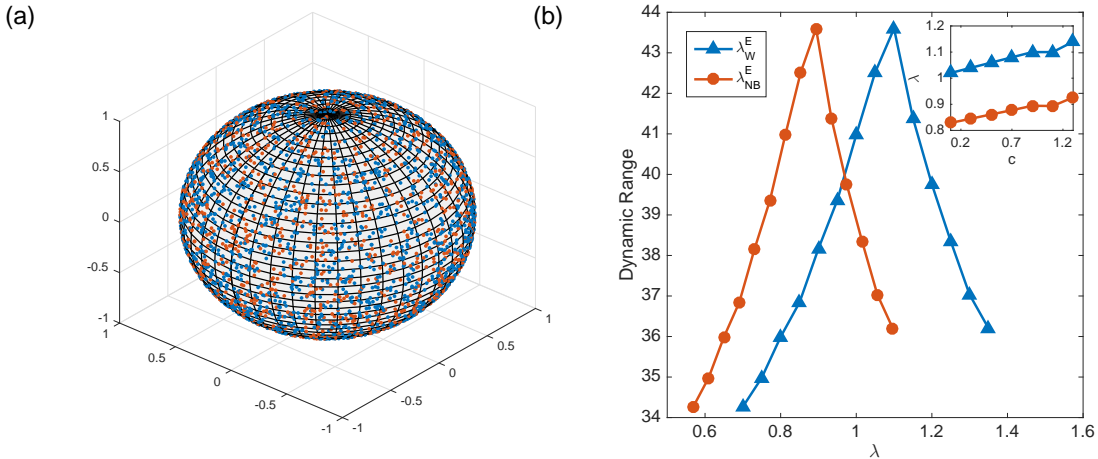


FIG. 9. (a) Generation of the synthetic neural network. 3,000 excitatory nodes (blue) and 2,000 inhibitory nodes (red) are uniformly placed on the surface of a unit sphere. (b) Relationship between the dynamic range and λ_W^E and λ_{NB}^E for a synthetic neural network ($N_e = 3,000$, $N_i = 2,000$, $c = 1$, the degree distribution follows a normal distribution with a mean of 9 and a variance of 1). We vary link weights to change the state of the system, and calculate the dynamic range, λ_W^E and λ_{NB}^E for each setting. At the critical state where the dynamic range is maximized, we find $\lambda_{NB}^E < 1$ and $\lambda_W^E > 1$, which agrees with our hypothesis. Inset shows the values of λ_W^E and λ_{NB}^E at the critical state for an increasing inhibition strength c .

findings highlight the important role of backtracking activation in excitable dynamics.

Critical behavior is common in biological systems [44]. Besides the commonly addressed neuronal networks, fingerprint of criticality have been reported for calcium signaling in myocytes [45], excitable beta cells [46], oocytes [47], etc. The operation of these biological systems near critical states may be crucial for their proper functioning. Certain inhibitory mechanisms exist in cells to regulate the dynamics of calcium signaling, which could be potentially relevant to our findings in this study. Further, several experimental studies on subcellular [48] as well as on the cellular level [49] echo our findings that the refractory periods are important in excitable dynamics. Another relevant field is the study on pacemaker activities induced by intracellular calcium waves, which has been found essential in the interstitial cell of Cajal (ICC) in the gastrointestinal tract and cardiac pacemaker cells in the heart. It has been shown that refractory phases are crucial to prevent backtracking of activations in systems guided by pacemaker activities [50, 51]. Findings in this study may

find applications in these biological systems in future works. It also merits further study whether imposing inhibition on influencers of excitable dynamics would result in efficient regulation of model dynamics [52, 53].

DATA ACCESSIBILITY

No real-world data were used in this study.

AUTHORS' CONTRIBUTIONS

R.Z. and S.P. designed the study. R.Z. and G.Q. wrote the code, ran simulations and performed the analysis. S.P. wrote the first draft of the manuscript. R.Z., G.Q. and J.W. reviewed and edited the manuscript.

COMPETING INTERESTS

We declare we have no competing interests.

FUNDING

This work was supported by the National Natural Science Foundation of China (11801058), the Fundamental Research Funds for the Central Universities (DUT18RC(4)066) and Beijing Natural Science Foundation (1192012, Z180005).

-
- [1] Kinouchi O, Copelli M. 2006 Optimal dynamical range of excitable networks at criticality. *Nat. Phys.* **2**, 348-351. (doi:10.1038/nphys289)
 - [2] Copelli M, Oliveira RF, Roque AC, Kinouchi O. 2005 Signal compression in the sensory periphery. *Neurocomputing* **65-66**, 691-696. (doi:https://doi.org/10.1016/j.neucom.2004.10.099)
 - [3] Gollo LL, Kinouchi O, Copelli M. 2009 Active dendrites enhance neuronal dynamic range. *PLoS Comput. Biol.* **5**, e1000402. (doi:10.1371/journal.pcbi.1000402)

- [4] Gollo LL, Copelli M, Roberts JA. 2016 Diversity improves performance in excitable networks. *PeerJ* **4**, e1912. (doi:10.7717/peerj.1912)
- [5] Wang CY, Wu ZX, Chen MZ. 2017 Approximate-master-equation approach for the Kinouchi-Copelli neural model on networks. *Phys. Rev. E* **95**, 012310 . (doi:10.1103/physRevE.95.012310)
- [6] Kinouchi O, Brochini L, Costa AA, Campos JGF, Copelli M. 2019 Stochastic oscillations and dragon king avalanches in self-organized quasi-critical systems. *Sci. Rep.* **9**, 3874. (doi:10.1038/s41598-019-40473-1)
- [7] Gautam SH, Hoang TT, McClanahan K, Grady SK, Shew WL. 2015 Maximizing sensory dynamic range by tuning the cortical state to criticality. *PLoS Comput. Biol.* **11**, e1004576. (doi:10.1371/journal.pcbi.1004576)
- [8] Williams-García RV, Moore M, Beggs JM, Ortiz G. 2014 Quasicritical brain dynamics on a nonequilibrium Widom line. *Phys. Rev. E* **90**, 062714.(doi:10.1103/PhysRevE.90.062714)
- [9] Marro J, Mejias JF, Pinamonti G, Torres JJ. 2013 Signal transmission competing with noise in model excitable brains. *AIP Conference Proceedings* **1510**, 85. (doi:10.1063/1.4776504)
- [10] Karrer B, Newman ME. 2011 Competing epidemics on complex networks. *Phys. Rev. E* **84**, 036106. (doi:10.1103/PhysRevE.84.036106)
- [11] Van Mieghem P. 2012 Epidemic phase transition of the SIS type in networks. *EPL* **97**, 48004. (doi:10.1209/0295-5075/97/48004)
- [12] Dodds PS, Harris KD, Danforth CM. 2013 Limited imitation contagion on random networks: Chaos, universality, and unpredictability. *Phys. Rev. Lett.* **110**, 158701. (doi:10.1103/PhysRevLett.110.158701)
- [13] Pei S, Tang S, Zheng Z. 2015 Detecting the influence of spreading in social networks with excitable sensor networks. *PLoS ONE* **10**, e0124848. (doi:10.1371/journal.pone.0124848)
- [14] Larremore DB, Shew WL, Restrepo JG. 2011 Predicting criticality and dynamic range in complex networks: effects of topology. *Phys. Rev. Lett.* **106**, 058101. (doi:10.1103/PhysRevLett.106.058101)
- [15] Larremore DB, Shew WL, Ott E, Restrepo JG. 2011 Effects of network topology, transmission delays, and refractoriness on the response of coupled excitable systems to a stochastic stimulus. *Chaos* **21**, 025117. (doi:10.1063/1.3600760)

- [16] Copelli M, Kinouchi O. 2005 Intensity coding in two-dimensional excitable neural networks. *Physica A* **349**, 431-442. (doi:https://doi.org/ 10.1016/j.physa.2004.10.043)
- [17] Zhang R, Pei S. 2018 Dynamic range maximization in excitable networks. *Chaos* **28**, 013103. (doi:10.1063/1.4997254)
- [18] Adini Y, Sagi D, Tsodyks M. 1997 Excitatory-inhibitory network in the visual cortex: Psychophysical evidence. *Proc. Natl. Acad. Sci. USA* **94**, 10426. (doi:10.1073/pnas.94.19.10426)
- [19] Park C, Terman D. 2010 Irregular behavior in an excitatory-inhibitory neuronal network. *Chaos* **20**, 023122. (doi:10.1063/1.3430545)
- [20] Folias SE, Ermentrout GB. 2011 New patterns of activity in a pair of interacting excitatory-inhibitory neural fields. *Phys. Rev. Lett.* **107**, 228103. (doi:10.1103/PhysRevLett.107.228103)
- [21] Pei S, Tang S, Yan S, Jiang S, Zhang X, Zheng Z. 2012 How to enhance the dynamic range of excitatory-inhibitory excitable networks. *Phys. Rev. E* **86**, 021909. (doi:10.1103/PhysRevE.86.021909)
- [22] Larremore DB, Shew WL, Ott E, Sorrentino F, Restrepo JG. 2014 Inhibition causes ceaseless dynamics in networks of excitable nodes. *Phys. Rev. Lett.* **112**, 138103. (doi:10.1103/PhysRevLett.112.138103)
- [23] Mongillo G, Rumpel S, Loewenstein Y. 2018 Inhibitory connectivity defines the realm of excitatory plasticity. *Nat. Neurosci.* **21**, 1463-1470. (doi:10.1038/s41593-018-0226-x)
- [24] Soriano J, Martínez MR, Tlusty T, Moses E. 2008 Development of input connections in neural cultures. *Proc. Natl. Acad. Sci. USA* **105**, 13758-13763. (doi:10.1073/pnas.0707492105)
- [25] Molloy M, Reed B. 1995 A critical point for random graphs with a given degree sequence. *Random Struct. Algor.* **6**, 161-180. (doi:10.1002/rsa.3240060204)
- [26] Stefanescu RA, Jirsa VK. 2008 A low dimensional description of globally coupled heterogeneous neural networks of excitatory and inhibitory neurons. *PLoS Comput. Biol.* **4**, e1000219. (doi:10.1371/journal.pcbi.1000219)
- [27] Copelli M, Roque AC, Oliveira RF, Kinouchi O. 2002 Physics of psychophysics: Stevens and Weber-Fechner laws are transfer functions of excitable media. *Phys. Rev. E* **65**, 060901. (doi:10.1103/PhysRevE.65.060901)
- [28] Newman M. E. J. 2002 Spread of epidemic disease on networks. *Phys. Rev. E* **66**, 016128. (doi:10.1103/PhysRevE.66.016128)

- [29] Mezard M, Montanari A. 2009 *Information, Physics, and Computation*. Oxford, UK: Oxford University Press.
- [30] Morone F, Makse HA. 2015 Influence maximization in complex networks through optimal percolation. *Nature* **524**, 65. (doi:10.1038/nature14604 <https://www.nature.com/articles/nature14604#supplementary-information>)
- [31] Pei S, Teng X, Shaman J, Morone F, Makse HA. 2017 Efficient collective influence maximization in cascading processes with first-order transitions. *Sci. Rep.* **7**, 45240. (doi:10.1038/srep45240)
- [32] Melnik S, Hackett A, Porter MA, Mucha PJ, Gleeson JP. 2011 The unreasonable effectiveness of tree-based theory for networks with clustering. *Phys. Rev. E* **83**, 036112. (doi:10.1103/PhysRevE.83.036112)
- [33] Hashimoto K. 1989 Zeta functions of finite graphs and representations of p-adic groups. In *Automorphic Forms and Geometry of Arithmetic Varieties (eds K Hashimoto, Y Namikawa)*, pp. 211-280. Academic Press.
- [34] Martin T, Zhang X, Newman ME. 2014 Localization and centrality in networks. *Phys. Rev. E* **90**, 052808. (doi:10.1103/PhysRevE.90.052808)
- [35] Karrer B, Newman ME, Zdeborová L. 2014 Percolation on sparse networks. *Phys. Rev. Lett.* **113**, 208702. (doi:10.1103/PhysRevLett.113.208702)
- [36] Hamilton KE, Pryadko LP. 2014 Tight lower bound for percolation threshold on an infinite graph. *Phys. Rev. Lett.* **113**, 208701. (doi:10.1103/PhysRevLett.113.208701)
- [37] Teng X, Pei S, Morone F, Makse HA. 2016 Collective influence of multiple spreaders evaluated by tracing real information flow in large-scale social networks. *Sci. Rep.* **6**, 36043. (doi:10.1038/srep36043)
- [38] Wang J, Pei S, Wei W, Feng X, Zheng Z. 2018 Optimal stabilization of Boolean networks through collective influence. *Phys. Rev. E* **97**, 032305. (doi:10.1103/PhysRevE.97.032305)
- [39] Wang J, Zhang R, Wei W, Pei S, Zheng Z. 2019 On the stability of multilayer Boolean networks under targeted immunization. *Chaos* **29**, 013133. (doi:10.1063/1.5053820)
- [40] Aleja D, Criado R, del Amo AJG, Pérez Á, Romance M. 2019 Non-backtracking PageRank: From the classic model to hashimoto matrices. *Chaos, Solitons & Fractals* **126**, 283-291. (doi:10.1016/j.chaos.2019.06.017)
- [41] Saad Y. 2011 *Numerical Methods for Large Eigenvalue Problems*. Philadelphia, US: SIAM.

- [42] Markram H, Toledo-Rodriguez M, Wang Y, Gupta A, Silberberg G, Wu C. 2004 Interneurons of the neocortical inhibitory system. *Nat. Rev. Neurosci.* **5**, 793. (doi:10.1038/nrn1519)
- [43] Wiles L, Gu S, Pasqualetti F, Parvesse B, Gabrieli D, Bassett DS, Meaney DF. 2017 Autaptic connections shift network excitability and bursting. *Sci. Rep.* **7**, 44006. (doi:10.1038/srep44006)
- [44] Muñoz MA. 2018 Colloquium: Criticality and dynamical scaling in living systems. *Rev. Mod. Phys.* **90**, 031001. (doi:10.1103/RevModPhys.90.031001)
- [45] Nivala M, Ko CY, Nivala M, Weiss JN, Qu Z. 2012 Criticality in intracellular calcium signaling in cardiac myocytes. *Biophys. J.* **102**, 2433-2442. (doi:10.1016/j.bpj.2012.05.001)
- [46] Stožer A, Markovič R, Dolensšek J, Perc M, Slak Rupnik M, Marhl M, Gosak M. 2019 Heterogeneity and delayed activation as hallmarks of self-organization and criticality in excitable tissue. *Front. Psychol.* **10**, 869. (doi:10.3389/fphys.2019.00869)
- [47] Lopez L, Piegari E, Sigaut L, Ponce Dawson S. 2012 Intracellular calcium signals display an avalanche-like behavior over multiple lengthscales. *Front. Psychol.* **3**, 350. (doi:10.3389/fphys.2012.00350)
- [48] Thul R, Coombes S, Roderick HL, Bootman MD. 2012 Subcellular calcium dynamics in a whole-cell model of an atrial myocyte. *Proc. Natl. Acad. Sci. USA* **109**, 2150-2155. (doi:10.1073/pnas.1115855109)
- [49] Schuster S, Marhl M, Höfer T. 2002 Modelling of simple and complex calcium oscillations: From singlecell responses to intercellular signalling. *Eur. J. Biochem.* **269**, 1333-1355. (doi:10.1046/j.0014-2956.2001.02720.x)
- [50] Gosak M, Marhl M, Perc M. 2009 Pacemaker-guided noise-induced spatial periodicity in excitable media. *Physica D* **238**, 506-515. (doi:10.1016/j.physd.2008.11.007)
- [51] Means SA, Sneyd J. 2010 Spatio-temporal calcium dynamics in pacemaking units of the interstitial cells of Cajal. *J. Theor. Biol.* **267**, 137-152. (10.1016/j.jtbi.2010.08.008)
- [52] Pei S, Wang J, Morone F, Makse HA. 2019 Influencer identification in dynamical complex systems. *J. Complex Netw.* In Press.
- [53] Pei S, Morone F, Makse HA. 2018 Theories for influencer identification in complex networks. In *Complex Spreading Phenomena in Social Systems* pp. 125-148. Springer, Cham. (doi:10.1007/978-3-319-77332-2_8)